Eur. Phys. J. Plus (2025) 140:497
https://doi.org/10.1140/epjp/s13360-025-06447-1

THE EUROPEAN PHYSICAL JOURNAL PLUS

Regular Article

Atomistic studies of helium trapping and diffusion at Ni–graphene interfaces

Hai Huang[1,a], **Xiaoxin Ge**[1], **Xu Yu**[1,2], **Yanxin Jiang**[1], **Qing Peng**[3]

[1] Key Laboratory of Material Physics, Ministry of Education, School of Physics, Zhengzhou University, Zhengzhou 450001, China
[2] International Joint Laboratory for Integrated Circuits Design and Application, Ministry of Education, School of Physics, Zhengzhou University, Zhengzhou 450001, China
[3] State Key Laboratory of Nonlinear Mechanics, Institute of Mechanics, Chinese Academy of Sciences, Beijing 100190, China

Received: 31 December 2024 / Accepted: 17 May 2025

Abstract The use of metal–nanocarbon interfaces to prevent the bubble-to-void transition has emerged as a novel approach for developing materials resistant to helium (He) embrittlement. However, many critical mechanisms governing He dynamics near these interfaces remain inadequately understood. Here we employed the Ni−graphene interface (NGI) as a model system to investigate He trapping and diffusion through atomistic simulations (300–1,200 K). Key findings demonstrate rapid He trapping at NGIs, with anisotropic in-plane diffusion ($[\bar{1}10]$, $[\bar{1}\bar{1}2]$) exhibiting a tenfold higher diffusivity (prefactor: 6.251×10^{-2} nm^2·ps^{-1}) and lower activation energy (0.057 eV) than pure Ni. Above 600 K, interfacial capture dominates, minimizing bulk residence. Unlike hydrogen, which forms stable C–H bonds, He migrates freely along NGIs without chemical interaction, promoting release. NGIs could suppress 3D bubble growth by redirecting He into planar pathways, aligning with observed bubble size reduction. The work contrasts He dynamics at NGIs versus grain boundaries, highlighting the superior capacity of metal–nanocarbon interfaces for He venting. These insights provide a mechanistic basis for designing helium-resistant composites, advancing strategies to mitigate embrittlement through controlled helium transport.

1 Introduction

In nuclear reactors, helium (He) produced through (n, α) reactions significantly impacts the performance of metallic structural materials [1, 2]. Due to its extremely low solubility, He atoms tend to coalesce into small bubbles, which serve as nucleation sites for void growth under irradiation-induced vacancy supersaturation. Consequently, this process leads to material swelling and He embrittlement at elevated temperatures [1–4]. Moreover, implanted He atoms can cause blistering and irradiation hardening [5–8], which further complicates the use of these materials in reactor environments. Generally, large voids, rather than smaller bubbles, are primarily responsible for the detrimental effects. To delay the transition of bubbles into voids, two strategies are widely adopted [9, 10]. The first involves creating more nucleation sites for He bubbles. The second aims to increase the critical bubble size required for voids to form. Unfortunately, neither approach does halt void formation or coalescence but aims to postpone the bubble-to-void transition, thereby mitigating the damaging effects of He-induced embrittlement [9, 10].

Recently, an alternative strategy has been proposed, in which carefully engineered metal–nanocarbon interfaces can shift the growth behavior of He precipitates from their conventional three-dimensional nanobubble formation to the more favorable creation of elongated one- or two-dimensional nanochannels [10–18]. For instance, Li et al. [11, 12] demonstrated, through both experiments and simulations, that the hollow spaces within carbon nanotubes can serve as "nano-chimneys" for He diffusion, thereby reducing the formation of He bubbles in the matrix. Si et al. [13] reported that W–graphene nanolayers with small-period thicknesses exhibit enhanced radiation tolerance, leading to a reduction in He bubble density. Furthermore, Huang et al. [14] discovered that Ni−graphene interfaces (NGIs) effectively trap He clusters by lowering formation energies and diffusion barriers, resulting in the significant segregation of planar He clusters at these interfaces. Collectively, these studies suggest that when one- or two-dimensional He nanochannels become interconnected, they may create a three-dimensional network. This network could allow He to escape from the material during prolonged exposure, thereby lowering its overall concentration. However, how He behaves at metal-nanocarbon interfaces is still not fully understood. Further research is needed to optimize materials for practical applications and predict long-term aging effects.

Understanding the mechanisms governing the migration and interaction of He atoms with metal–nanocarbon interfaces presents a challenging, multifaceted issue. This problem spans multiple scales, from atomic-level processes to macroscopic phenomena. It involves both spatial and temporal dimensions. To address it effectively, researchers must combine experimental methods with

[a] e-mail: huanghai@zzu.edu.cn (corresponding author)

Published online: 06 June 2025

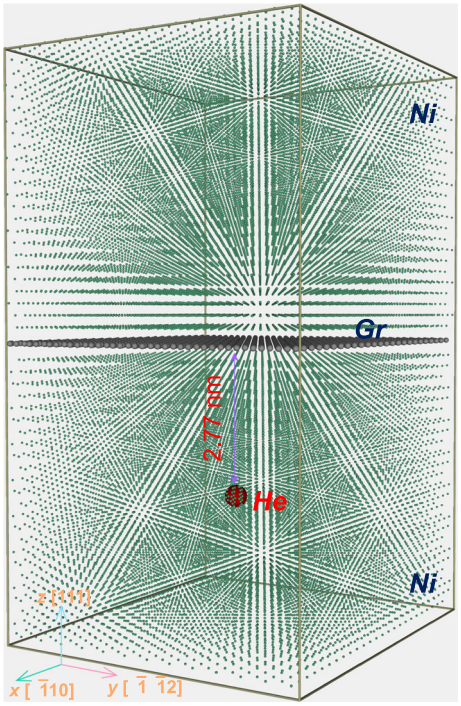

Fig. 1 NGI model featuring a solute He atom positioned 2.77 nm from the graphene layer

computational modeling. Among them, a key aspect is the determination of essential parameters governing He diffusion, clustering, and its interaction with interfaces [3, 4, 10, 11, 19]. Due to the challenges in experimentally detecting individual He atoms, atomistic simulations remain the most suitable approach for studying He diffusion dynamics at metal–nanocarbon interfaces [10, 11, 20–22]. This method has been effective for decades. It provides atomic-scale insights into material processes, particularly those occurring at picosecond timescales and nanometer spatial scales. Researchers have successfully applied it to study a wide range of materials [3, 4, 11, 23, 24]. In this study, we utilized the NGI within a Ni−graphene nanocomposite (NGNC) as a model system to explore the trapping and diffusion of isolated He atoms nearby via molecular dynamics (MD) simulations. These thermodynamic simulations were conducted over a temperature range of 300 to 1,200 K, allowing for detailed observation of the dynamic evolution of He and the quantification of its diffusion characteristics. Nickel was selected as the matrix material due to its extensive use in nuclear reactors and its high (n, α) reaction cross section [14, 19, 24, 25].

2 Simulation methodology

All simulations were conducted utilizing the parallel MD software LAMMPS [26], with visualizations generated through OVITO code [27]. This study also used the sandwich NGI model, which was developed in prior work [14, 24]. The model contains 32,500 atoms and has dimensions of $6.21 \times 5.59 \times 10.10$ nm^3 (see Fig. 1). The interactions among Ni–Ni, C–C, He–He, and Ni–He were characterized using the embedded atom method (EAM) potential [28], the adaptive intermolecular reactive empirical bond order (AIREBO) potential [29], the Beck potential [30], and the Morse-3G interatomic potential [31], respectively. Furthermore, the interactions between Ni–C and He–C were represented through the Lennard–Jones potential [32, 33]. The parameters for each potential, along with the construction and optimization of the NGI model, have been detailed in prior works [14]. To initiate the process, a solute He atom was randomly inserted into the system at an interstitial site, located 2.77 nm from the graphene layer (see Fig. 1). Following energy minimization, the NGI–He system underwent thermal relaxation for 5.0 ns at a specified temperature. The Nose–Hoover isobaric-isothermal (NPT) ensemble was adopted to maintain stable system pressure throughout the simulation. The thermostat temperature was adjusted within the range of 300 to 1,200 K to investigate the temperature dependence of He diffusion properties.

3 Results and discussion

Figure 2 shows how a single He atom moves near the NGI at various temperatures. The trajectories track the position of the atom from 0 to 5.0 ns. These paths were plotted every 10.0 ps and linked sequentially to visualize the full motion. At 300 K, the solute He became trapped in the NGI after a complex, long-distance migration through the bulk. At 500 K, solute He moves much farther

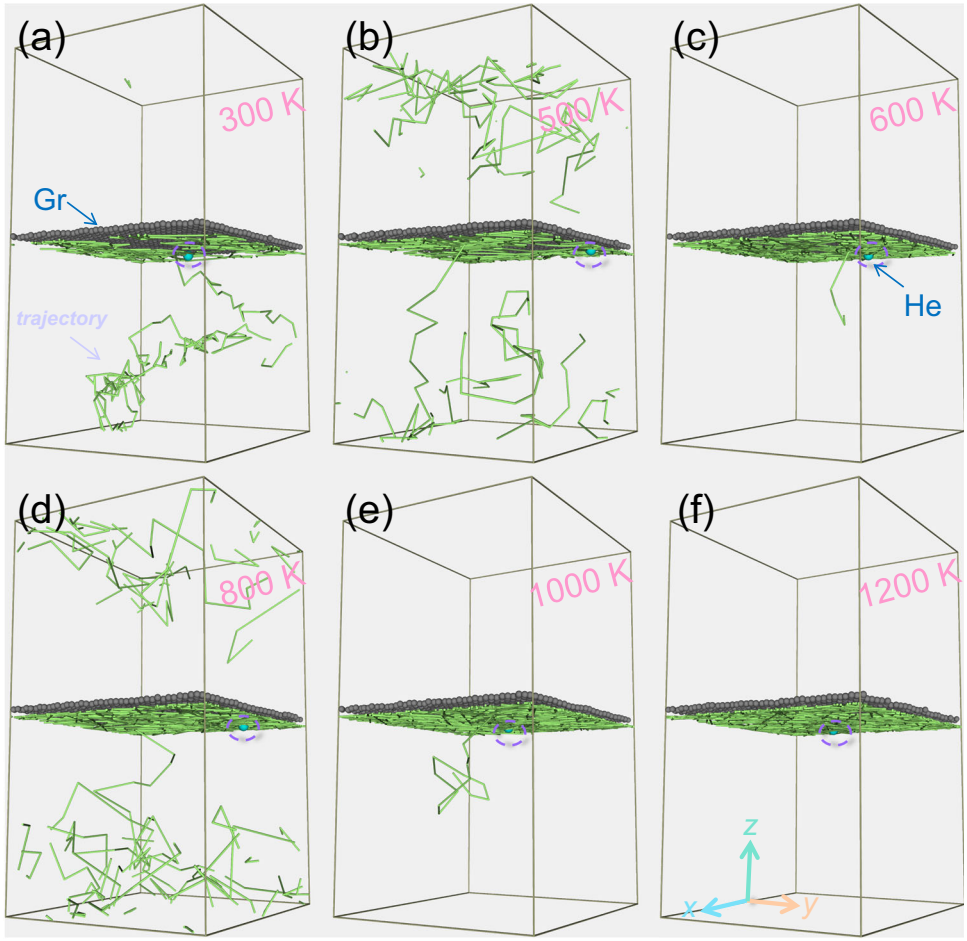

Fig. 2 MD trajectories of a single He atom diffusing near an NGI at different temperatures over a 5.0 ns simulation period: **a** 300 K, **b** 500 K, **c** 600 K, **d** 800 K, **e** 1,000 K, and **f** 1,200 K. The trajectories illustrate the temperature-dependent mobility and spatial distribution of the He atom

through the material. Both individual jumps and overall diffusion distances increase significantly. This increased mobility allows He atoms to cross the entire simulation box, reaching the opposite side. At 600 K, He swiftly enters the NGI with minimal disruption. Below 600 K, the diffusion of He in the bulk differs significantly from hydrogen (H). Solute H shows limited movement, staying close to its starting position and being less affected by the NGI [34]. In contrast, solute He moves much more freely through the Ni matrix. This difference arises because the migration energy of He in the bulk is much lower than that of H, which facilitates its movement [14, 34]. Unexpectedly, at 800 K, the diffusion behavior of He resembles that at 500 K, characterized by convoluted migration through the bulk. As the temperature rises, the total diffusion distance gradually decreases, and He is rapidly captured by the interface, showing minimal bulk diffusion. Overall, He is eventually captured by the interface between 300 and 1,200 K, yet its residence time in the bulk shows no clear temperature dependence. This lack of dependence may arise from inconsistent migration pathways of He at different temperatures. Once He reaches the NGI, both its diffusion frequency and distance increase with temperature, indicating little resistance to He diffusion at the interface. This contrasts with H, which forms C−H bonds with carbon, hindering its interface migration [34]. He, however, is difficult to confine. It tends to move across the interface, which may result in its release from the material. This supports the hypothesis that NGIs may act as two-dimensional nanochannels for He.

During the thermal relaxation process, the positions of solute He were continuously tracked over time. The mean square displacement (MSD) of a single He atom was computed based on its total diffusion distance, using the following equation

$$MSD = [r(t_0 + t) - r(t_0)]^2, \tag{1}$$

where $r(t_0)$ and $r(t_0 + t)$ denote the initial and instantaneous positions of atoms at time t_0 and $t_0 + t$, with $\langle \ldots \rangle$ referring to the ensemble average. Analysis of the computational trajectories allows for a clear understanding of solute He diffusion behavior near the NGI. Figure 3(a) presents the MSDs of a single He atom near the NGI at various temperatures. The MSDs generally increase with time at temperatures not exceeding 600 K, consistent with observations from similar studies [24, 35, 36]. Above 600 K, the pattern changes. The MSDs no longer follow a regular trend. Instead, they fluctuate unpredictably, rising and falling without a clear pattern. This inconsistency likely arises from the dynamic processes at elevated temperatures, where Ni or C atoms occasionally undergo jumps and then can significantly alter the movement of He [36]. The MSD peak increases with temperature up to 600 K, where it reaches its maximum. After declining, it suddenly rises again at 1,200 K. This pattern suggests that random atomic vibrations caused

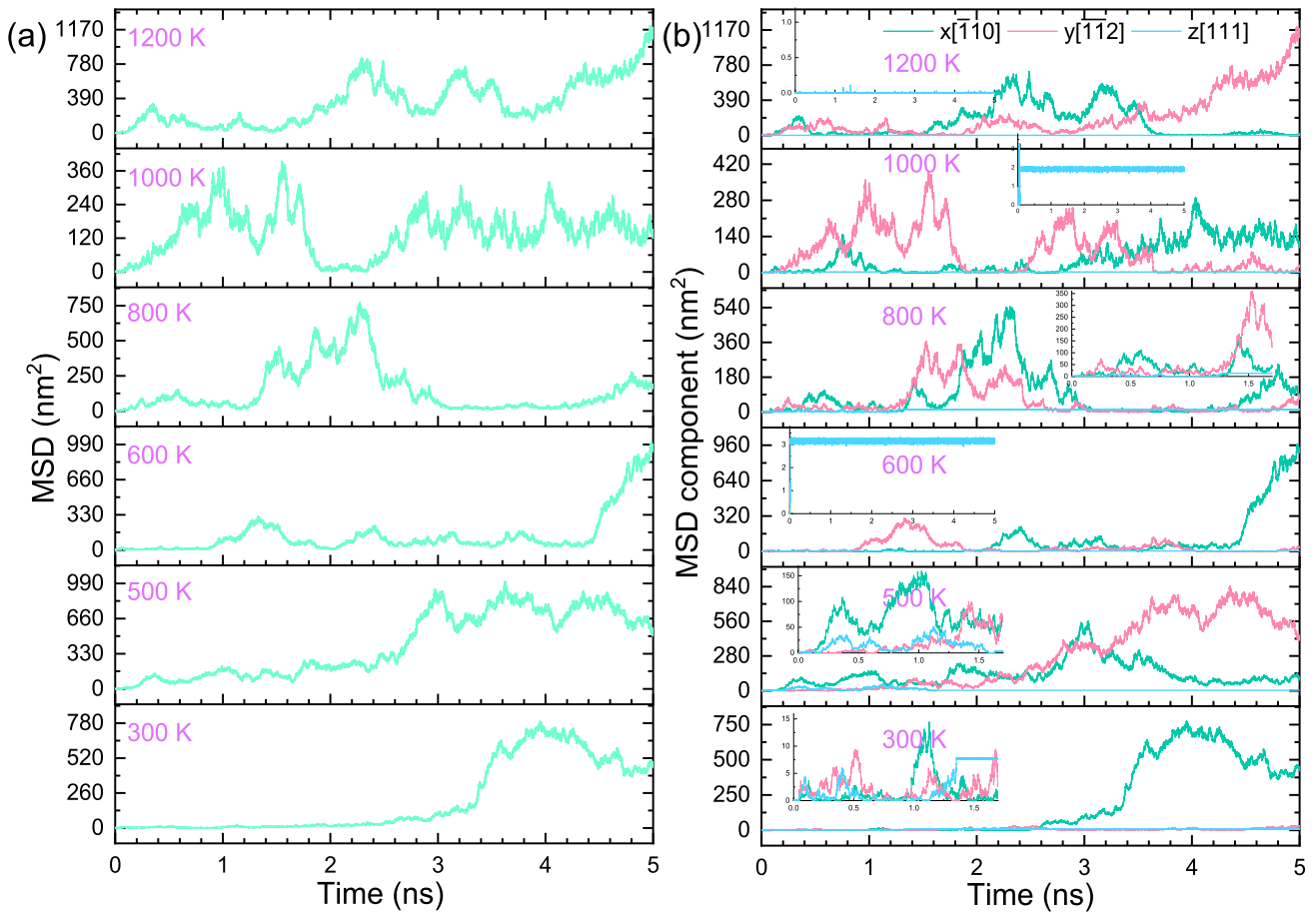

Fig. 3 **a** MSDs and **b** their directional components along principal crystallographic axes for a single He atom within NGNC, simulated over 5.0 ns at temperatures ranging from 500 to 1,200 K. The MSD curves quantify the diffusive behavior, while the axial components reveal anisotropic mobility trends

by high temperature restrict He diffusion in NGNC. Regardless of temperature, solute He demonstrates a random walk, making its MSDs difficult to stabilize over extended periods. The diffusion behavior near NGIs resembles that observed at small-angle grain boundaries (GBs), yet differs from large-angle GBs with high dislocation densities [22, 37, 38]. For example, Hammond et al. [37] reported that in tungsten, He diffusion is initially biased toward GBs. However, their movement becomes limited when they reach specific boundaries, such as $\sum 3 < 111 > \{211\}$ or $\sum 5 < 100 > \{310\}$. This restriction is especially strong for motion perpendicular to the GBs.

The MSD can be broken down into its x, y, and z components, as shown in Fig. 3(b). Before becoming trapped at the interface (observed at 300, 500, and 800 K), the solute He in the bulk exhibits two-dimensional diffusion. This movement occurs mainly in the xy-plane, with greater migration along the $[\bar{1}10]$ direction. Notably, this diffusion pattern shows no significant temperature dependence. This behavior contrasts with findings from studies on Fe- or W-GBs [22, 36], where He diffusion in the bulk transitions from one to two or even three dimensions as the temperature rises. This variation may stem from temperature-induced changes in the migration pathways of solute He in the bulk of polycrystalline [22, 36]. For example, in the case of W-GBs, below 300 K, He diffuses directly between neighboring tetrahedral interstitial sites (TIS) in the bulk, while at higher temperatures, migration follows a mix of TIS–TIS and TIS–octahedral interstitial site (OIS)–TIS pathways [22]. In contrast, our prior simulations indicated that in the bulk of NGNC, He atoms prefer the TIS–OIS–TIS pathway over the TIS–TIS pathway [14]. Once a He atom approaches approximately 1.10 nm from the NGI [14], it becomes effectively "locked" at the interface and remains confined there. He atoms captured at the interface exhibit either predominantly one-dimensional diffusion (*e.g.*, at 300 and 600 K) or two-dimensional diffusion (*e.g.*, at 500 and 800 K), with no clear temperature dependence. Additionally, He diffuses much more rapidly at the NGI than in the bulk, primarily due to the lower diffusion barrier at the interface [14]. As a result, He atoms demonstrate high mobility within the NGI, and the interface facilitates rapid diffusion pathways for He along specific directions [14].

The MSD analysis mentioned above can also be employed to determine the solute He diffusion coefficients in the NGNC system at varying temperatures. Utilizing the Einstein relation, the self-diffusivity of He at a given temperature can be calculated below

$$D = \frac{1}{2d} \lim_{t \to \infty} \frac{MSD}{t}, \tag{2}$$

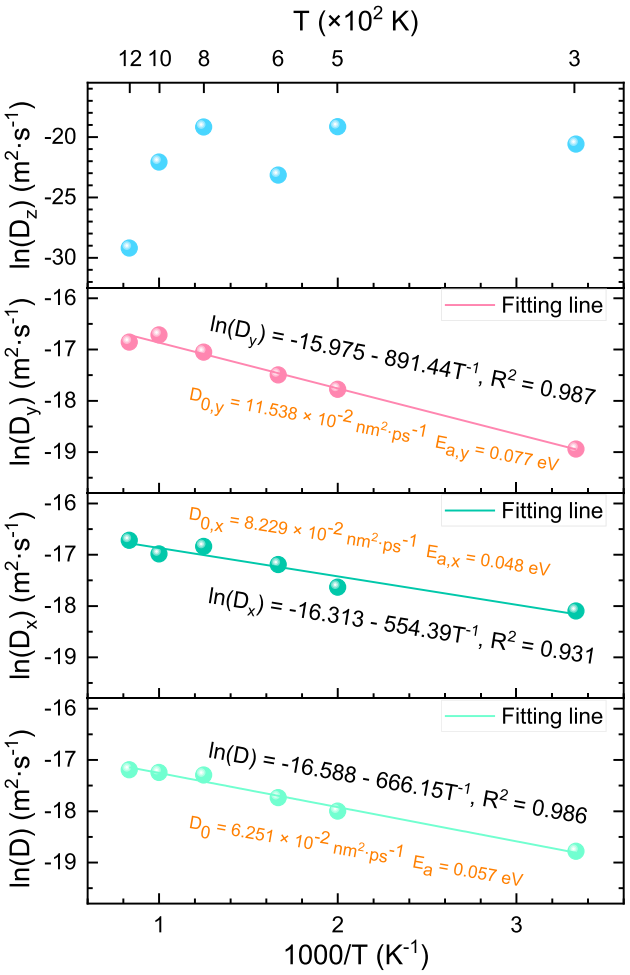

Fig. 4 Temperature-dependent diffusion coefficients of a single He atom within NGNC, including directional components along the principal crystallographic axes. The data quantify the thermally activated diffusion anisotropy and overall mobility of He within the NGNC

where the dimensionality, d, represents one-, two-, or three-dimensional diffusion of solute He, corresponding to $d = 1$, 2, or 3, respectively. Once the diffusion coefficients are determined for different temperatures, the activation energy (E_a) for He diffusion can be derived using the Arrhenius equation

$$\mathrm{D} = \mathrm{D_0}\exp\left(-\frac{\mathrm{E_a}}{\mathrm{k_\beta T}}\right), \tag{3}$$

where D_0 is the pre-exponential factor, and k_β is the Boltzmann constant. The temperature dependence of diffusivity (plotted as ln(D)–1000/T) for He at the range of 300 to 1,200 K is shown in Fig. 4, along with the activation energy and pre-exponential factor. All MD data points, except for the z-component, show good agreement with the linear Arrhenius plots, suggesting high simulation convergence. The calculated prefactor and activation energy for He diffusion is 6.251×10^{-2} nm^2·ps^{-1} and 0.057 eV, respectively. The prefactor is numerically an order of magnitude higher than that of pure Ni calculated by Torres et al. [39] using the same EAM potential, while the activation energy is an order of magnitude smaller than that of pure Ni. This indicates that the presence of NGIs in the composite appears to enhance He diffusivity compared to pure Ni, accelerating He movement and potentially promoting its release through the interfaces. This finding may further explain the observed reduction in He bubble size within the NGNC compared to pure Ni [17]. The present D_0 aligns reasonably well with values reported for other interfaces such as Fe-GBs [35, 36]. The activation energy is marginally lower than prior results from the dimer method [14], with similar trends reported by Deng et al. [35]. It is crucial to note that the activation energy for He in the NGNC may not fully reflect the actual diffusion barrier. Instead, it serves as an effective value because NGI rapidly traps solute He. This trapping restricts its movement along the [111] direction. Additionally, He diffusion exhibits a higher prefactor in the $[\bar{1}12]$ direction compared to the $[\bar{1}10]$ direction, suggesting that the former, particularly within the NGI, supports faster He transport. The z-component of He diffusivity remains relatively unaffected by temperature, with some anomalies, such as a minimum value observed at 1,200 K. This behavior might result from varying disturbances in the spacing between the graphene and Ni layers caused by temperature. Unlike GBs, where out-of-plane diffusion remains feasible despite reduced diffusivity due to high-density dislocations [35, 36], He atoms find it harder to escape from the NGIs.

4 Conclusions

In summary, this study has explored the influence of NGIs on He trapping and diffusion characteristics, employing atomistic simulations. Below 600 K, He undergoes long-range bulk diffusion before interfacial capture, while above 600 K, rapid interfacial trapping limits its bulk migration. Notably, He exhibits significantly higher mobility in the NGNC compared to H, due to its lower migration energy. Elevated temperatures (≥ 800 K) induce erratic atomic vibrations, reducing the bulk residence time of He but accelerating its migration at the interface. He diffusion in the bulk is primarily two-dimensional in the xy-plane, while at the NGI, it becomes one- or two-dimensional depending on temperature. He diffusion at the NGI is anisotropic, favoring in-plane ($[\bar{1}10]$,$[\bar{1}\bar{1}2]$) over out-of-plane ([111]) directions. The calculated activation energy for He diffusion (0.057 eV) is an order of magnitude lower than in pure Ni, with a prefactor (6.251×10^{-2} nm^2·ps^{-1}) tenfold higher, indicating enhanced He diffusivity due to the presence of NGI. Unlike H, He avoids chemical bonding at the NGI, enabling rapid interfacial transport and potential material release. These findings underscore that NGIs could serve as effective two-dimensional nanochannels for He release. The study enhances the understanding of He dynamics in metal–nanocarbon composites, revealing that optimizing nanocarbon dispersion within the metallic matrix can significantly prevent the bubble-to-void transition. This strategy may help mitigate He-induced embrittlement in metallic structural materials, thereby ensuring the reliable operation of nuclear reactors.

Acknowledgements This work was supported by the National Natural Science Foundation of China (Grant No. 12105249), the Young Talent Support Program of Henan Association for Science and Technology (Grant No. 2025HYTP047), the Key Project for Science and Technology Development of Henan Province (Grant No. 242102230052), the Henan Province Postdoctoral Science Foundation (Grant No. 202102012), and the National Supercomputing Center in Zhengzhou. Furthermore, we thank Bin Cai for help in the revision stage of the paper.

Data Availability Statement This manuscript has associated data in a data repository. [Authors' comment: The authors declare that the data and equations supporting the results of this study are available within the paper. The raw data sets generated during the current study are available from the corresponding author upon reasonable request.]

Declarations

Conflicts of interest The authors declare that they have no competing interests.

Ethical approval Not applicable.

References

1. S. Qiu, H. Liu, M. Jiang, S. Min, Y. Gu, Q. Wang, J. Yang, X. Li, Z. Chen, J. Hou, A brief review on He ion irradiation research of steel and iron-based alloys in nuclear power plants. Acta Metall. Sin. Engl. **36**, 529–551 (2023)
2. S. Li, J. Li, W. Han, Radiation-induced helium bubbles in metals. Materials **12**, 1036 (2019)
3. W. Zhang, H. Han, J. Dai, C. Ren, C. Wang, L. Yan, H. Huang, Z. Zhu, Simulation of migration and coalescence of helium bubbles in nickel. J. Nucl. Mater. **518**, 48–53 (2019)
4. I.C. Njifon, E. Torres, Effect of grain boundaries on the helium degradation mechanisms of alloy 800H: A molecular dynamics study. J. Nucl. Mater. **603**, 155395 (2025)
5. M.E. Bannister, F.W. Meyer, H. Hijazi, K.A. Unocic, L.M. Garrison, C.M. Parish, Surface morphologies of He-implanted tungsten. Nucl. Instrum. Meth. B **382**, 76–81 (2016)
6. K.D. Hammond, Helium, hydrogen, and fuzz in plasma-facing materials. Mater. Res. Express **4**, 104002 (2017)
7. K. Fukumoto, Y. Zou, T. Nagasaka, R. Ishigami, Microstructural changes and irradiation hardening behavior of V-4Cr-4Ti alloys irradiated with He ions using flash-electropolishing. J. Nucl. Mater. **603**, 155438 (2025)
8. T. Liu, X. Ge, F. Chen, Y. Jiang, X. Yu, H. Huang, An experimental study on corrosion resistance of Ti35 alloy and its high-fluence hydrogen irradiation damage behavior. J. Phys. Chem. Solids **201**, 112646 (2025)
9. Y. Wang, K. Hattar, Radiation damage in materials—Helium effects. Materials **13**, 2143 (2020)
10. Y. Yang, L. He, Y. Ni, Atomistic insight into the unique mechanism of helium management at FCC 111}//{111 FCC semi-coherent interfaces. Surf. Interfaces **52**, 104893 (2024)
11. R.I. González, F. Valencia, J. Mella, A.C.T. van Duin, K.P. So, J. Li, M. Kiwi, E.M. Bringa, Metal-nanotube composites as radiation resistant materials. Appl. Phys. Lett. **109**, 033108 (2016)
12. K.P. So, D. Chen, A. Kushima, M. Li, S. Kim, Y. Yang, Z. Wang, J.G. Park, Y.H. Lee, R.I. Gonzalez, M. Kiwi, E.M. Bringa, L. Shao, J. Li, Dispersion of carbon nanotubes in aluminum improves radiation resistance. Nano Energy **22**, 319–327 (2016)
13. S. Si, W. Li, X. Zhao, M. Han, Y. Yue, W. Wu, S. Guo, X. Zhang, Z. Dai, X. Wang, X. Xiao, C. Jiang, Significant radiation tolerance and moderate reduction in thermal transport of a tungsten nanofilm by inserting monolayer graphene. Adv. Mater. **29**, 1604623 (2017)
14. H. Huang, X. Tang, F. Gao, F. Chen, G. Ge, Y. Yan, Q. Peng, Release of helium-related clusters through a nickel–graphene interface: an atomistic study. Appl. Surf. Sci. **487**, 218–227 (2019)
15. K. Cui, Y. Zhao, Z. Yu, M. Yu, X. Li, X. Huang, J. Qiu, L. Sun, H. Zhao, N. Gao, K. Tai, C. Liu, Extraordinary radiation tolerance of a Ni nanocrystal-decorated carbon nanotube network encapsulated in amorphous carbon. J. Mater. Sci. Technol. **155**, 253–261 (2023)
16. H. Huang, X. Tang, K. Xie, Q. Peng, Enhanced self-healing of irradiation defects near a Ni–graphene interface by damaged graphene: Insights from atomistic modeling. J. Phys. Chem. Solids **151**, 109909 (2020)
17. H. Huang, X. Tang, F. Chen, J. Liu, X. Sun, L. Ji, Radiation tolerance of nickel-graphene nanocomposite with disordered graphene. J. Nucl. Mater. **510**, 1–9 (2018)

18. J. Tang, G. Wei, X. Cai, S. Hu, T. Shen, T. Cheng, R. Yin, J. Zhang, X. Ruan, B. Yang, Y. Wang, G. Cai, C. Jiang, F. Ren, Smart 3D network nanocomposites collect irradiation-induced "trash." Matter **3**, 1631–1645 (2020)
19. C. Wang, C. Ren, W. Zhang, H. Gong, P. Huai, Z. Zhu, H. Deng, W. Hu, A molecular dynamics study of helium diffusion and clustering in fcc nickel. Comp. Mater. Sci. **107**, 54–57 (2015)
20. Y. Hu, P. Huang, F. Wang, Nanopore graphene-tungsten composite with enhanced irradiated helium atoms storage capacity. J. Nucl. Mater. **574**, 154174 (2023)
21. M. Li, Q. Hou, J. Cui, M. Qiu, A. Yang, M. Zhou, Atomistic simulations of helium behavior at the Cu (111)/W (110) interface. J. Nucl. Mater. **555**, 153157 (2021)
22. Y. Feng, J. Shang, G. Lu, Migration and nucleation of helium atoms at (110) twist grain boundaries in tungsten. J. Nucl. Mater. **487**, 200–209 (2017)
23. L. Ma, T. Liu, B. Cai, Z. Liu, G. Zhang, J. Li, H. Li, H. Huang, Molecular dynamics studies of primary irradiation damage in α-type Ti35 alloy. Phys. Status Solidi B **260**, 2200560 (2023)
24. T. Liu, X. Yuan, H. Huang, Primary irradiation damage in Ni–graphene nanocomposites with pre-existing hydrogen: insights from atomistic simulations. Eur. Phys. J. Plus **139**, 22 (2024)
25. F. Ding, L. Zhou, L. Zhao, X. Dou, K. Xiao, J. Song, J. Du, G. Jiang, Theoretical study on the influence of Cr, Mo, and W alloying additions on the helium behavior in nickel. J. Nucl. Mater. **565**, 153720 (2022)
26. S. Plimpton, Fast parallel algorithms for short-range molecular dynamics. J. Comput. Phys. **117**, 1–19 (1995)
27. A. Stukowski, Visualization and analysis of atomistic simulation data with OVITO–the Open Visualization Tool. Model. Simul. Mater. Sci. **18**, 015012 (2009)
28. G. Bonny, N. Castin, D. Terentyev, Interatomic potential for studying ageing under irradiation in stainless steels: the FeNiCr model alloy. Model. Simul. Mater. Sci. **21**, 085004 (2013)
29. S.J. Stuart, A.B. Tutein, J.A. Harrison, A reactive potential for hydrocarbons with intermolecular interactions. J. Chem. Phys. **112**, 6472–6486 (2000)
30. D.E. Beck, A new interatomic potential function for helium. Mol. Phys. **14**, 311–315 (1968)
31. E. Torres, C. Judge, H. Rajakumar, A. Korinek, J. Pencer, G. Bickel, Atomistic simulations and experimental measurements of helium nano-bubbles in nickel. J. Nucl. Mater. **495**, 475–483 (2017)
32. S.P. Huang, D.S. Mainardi, P.B. Balbuena, Structure and dynamics of graphitesupported bimetallic nanoclusters. Surf. Sci. **545**, 163–179 (2003)
33. E. Jin, S. Du, M. Li, C. Liu, S. He, J. He, H. He, Influence of helium atoms on the shear behavior of the fiber/matrix interphase of SiC/SiC composite. J. Nucl. Mater. **479**, 504–514 (2016)
34. H. Huang, Q. Peng, X. Tang, Superior hydrogen permeation resistance via Ni–graphene nanocomposites: insights from atomistic simulations. J. Mater. Res. Technol. **28**, 2086–2097 (2024)
35. H. Deng, W. Hu, F. Gao, H.L. Heinisch, S. Hu, Y. Li, R.J. Kurtz, Diffusion of small He clusters in bulk and grain boundaries in α-Fe. J. Nucl. Mater. **442**, S667–S673 (2013)
36. F. Gao, H. Heinisch, R.J. Kurtz, Diffusion of He interstitials in grain boundaries in α-Fe. J. Nucl. Mater. **351**, 133–140 (2006)
37. K.D. Hammond, L. Hu, D. Maroudas, B.D. Wirth, Helium impurity transport on grain boundaries: enhanced or inhibited? EPL **110**, 52002 (2015)
38. X. Wang, L. Niu, S. Wang, Strong trapping and slow diffusion of helium in a tungsten grain boundary. J. Nucl. Mater. **487**, 158–166 (2017)
39. E. Torres, J. Pencer, D.D. Radford, Density functional theory-based derivation of an interatomic pair potential for helium impurities in nickel. J. Nucl. Mater. **479**, 240–248 (2016)